Short Article

Developmental Cell

The Ciliary Machinery Is Repurposed for T Cell Immune Synapse Trafficking of LCK

Highlights

- LCK immune synapse focusing requires its strong interaction with ciliary UNC119A
- ARL3^{Q71L} results in unfocused LCK localization and increased T cell stimulation
- The ciliary ARL3-GEF ARL13B localizes to the immune synapse
- UNC119A regulatory arm interacts with LCK kinase domain in a phosphoregulated manner

Authors

Louise A. Stephen, Yasmin ElMaghloob, Michael J. McIlwraith, Tamas Yelland, Patricia Castro Sanchez, Pedro Roda-Navarro, Shehab Ismail

Correspondence

s.ismail@beatson.gla.ac.uk

In Brief

Signaling proteins are focused at the immune synapse, where T cells form an interface with target cells. Stephen, ElMaghloob, and McIlwraith et al. demonstrate that T cells repurpose a mechanism used by the cilia, an organelle that T cells lack, to focus the signaling protein LCK at the immune synapse.

Stephen et al., 2018, Developmental Cell *47*, 122–132
October 8, 2018
https://doi.org/10.1016/j.devcel.2018.08.012

CellPress

CellPress

Developmental Cell
Short Article

The Ciliary Machinery Is Repurposed for T Cell Immune Synapse Trafficking of LCK

Louise A. Stephen,[1,5] Yasmin ElMaghloob,[1,4,5] Michael J. McIlwraith,[1,5] Tamas Yelland,[1] Patricia Castro Sanchez,[2,3] Pedro Roda-Navarro,[2,3] and Shehab Ismail[1,4,6,*]
[1]CR-UK Beatson Institute, Garscube Estate, Switchback Road, Glasgow G61 1BD, UK
[2]Department of Immunology, School of Medicine, Universidad Complutense de Madrid, Madrid 28040, Spain
[3]12 de Octubre Health Research Institute (imas12), Madrid 28040, Spain
[4]Institute of Cancer Sciences, University of Glasgow, Glasgow G12 8QQ, UK
[5]These authors contributed equally
[6]Lead Contact
*Correspondence: s.ismail@beatson.gla.ac.uk
https://doi.org/10.1016/j.devcel.2018.08.012

SUMMARY

Upon engagement of the T cell receptor with an antigen-presenting cell, LCK initiates TCR signaling by phosphorylating its activation motifs. However, the mechanism of LCK activation specifically at the immune synapse is a major question. We show that phosphorylation of the LCK activating Y394, despite modestly increasing its catalytic rate, dramatically focuses LCK localization to the immune synapse. We describe a trafficking mechanism whereby UNC119A extracts membrane-bound LCK by sequestering the hydrophobic myristoyl group, followed by release at the target membrane under the control of the ciliary ARL3/ARL13B. The UNC119A N terminus acts as a "regulatory arm" by binding the LCK kinase domain, an interaction inhibited by LCK Y394 phosphorylation, thus together with the ARL3/ARL13B machinery ensuring immune synapse focusing of active LCK. We propose that the ciliary machinery has been repurposed by T cells to generate and maintain polarized segregation of signals such as activated LCK at the immune synapse.

INTRODUCTION

T cell receptor (TCR) signaling takes place upon the interaction of the TCR with its cognate peptide-major histocompatibility complex (pMHC) on the antigen-presenting cell (APC). An initial event in TCR signaling is the phosphorylation of immunoreceptor tyrosine-based activation motifs (ITAMs) on the intracellular tails of the TCR by the lymphocyte-specific tyrosine protein kinase, LCK. LCK activity, similar to that of other SRC family kinases (SFKs), is regulated by the phosphorylation of two key tyrosine residues. Phosphorylation of tyrosine 394 in the activation loop increases its kinase activity, whereas phosphorylation of tyrosine 505 downregulates LCK activity (Boggon and Eck, 2004). There are four populations of LCK in T cells: active (pY394), inactive (pY505), primed (no phosphorylation), and double phosphorylated (pY394+pY505). Two models have been proposed to explain how TCR-pMHC binding initiates TCR signaling: (1) the "standby" model, where recognition of a pMHC does not increase the active LCK population but causes redistribution of active LCK or exposure of the ITAMs, which would result in the initiation of TCR signaling (Nika et al., 2010); and (2) the "de novo activation of LCK" model, where the active LCK population is increased upon recognition of a cognate pMHC (Ballek et al., 2015; Philipsen et al., 2017). Despite being crucial for LCK activity in cells, phosphorylation of tyrosine 394 *in vitro* results in only a 2-fold increase of kinase activity of LCK (Hui and Vale, 2014; Liaunardy-Jopeace et al., 2017). The "standby" model would require a highly regulated mechanism to prevent phosphorylation of ITAMs in the absence of a cognate pMHC, and the "de novo activation" model would require a mechanism that amplifies the impact of phosphorylating Y394. Although it has not been reported until now, both models suggest some crosstalk between LCK activation and its trafficking.

Following TCR signaling, T cells form immune synapses at the interface with APCs, where a canonical synapse comprises three concentric rings called supramolecular activation centers (SMAC): central supramolecular activation centers (cSMACs), peripheral supramolecular activation centers (pSMAC), and distal supramolecular activation centers (dSMAC) (Monks et al., 1998). Although the immune synapse is not enclosed in membranes, it still shows specific localization and retention of LCK (Ehrlich et al., 2002).

In this study, we propose a trafficking model where the ciliary UNC119A extracts and solubilizes LCK from membranes, which is then released by the small GTPase ARL3-GTP at the immune synapse where the ciliary ARL3 guanine nucleotide exchange factor (GEF) ARL13B is localized. The activation of LCK by autophosphorylation on tyrosine 394 disrupts the interaction of UNC119A with LCK and thus traps active LCK on the destination membrane. Our study describes a trafficking pathway for regulation of the SFK, LCK, which has profound implications for how T cells have co-opted the ciliary trafficking pathway to provide spatial control of signaling at the immune synapse.

RESULTS

UNC119A Shows a Strong Specificity for LCK

UNC119A has been reported to interact with several myristoylated SFK members (Cen et al., 2003), thus opening the question of whether specificity could be achieved in SFK regulation by

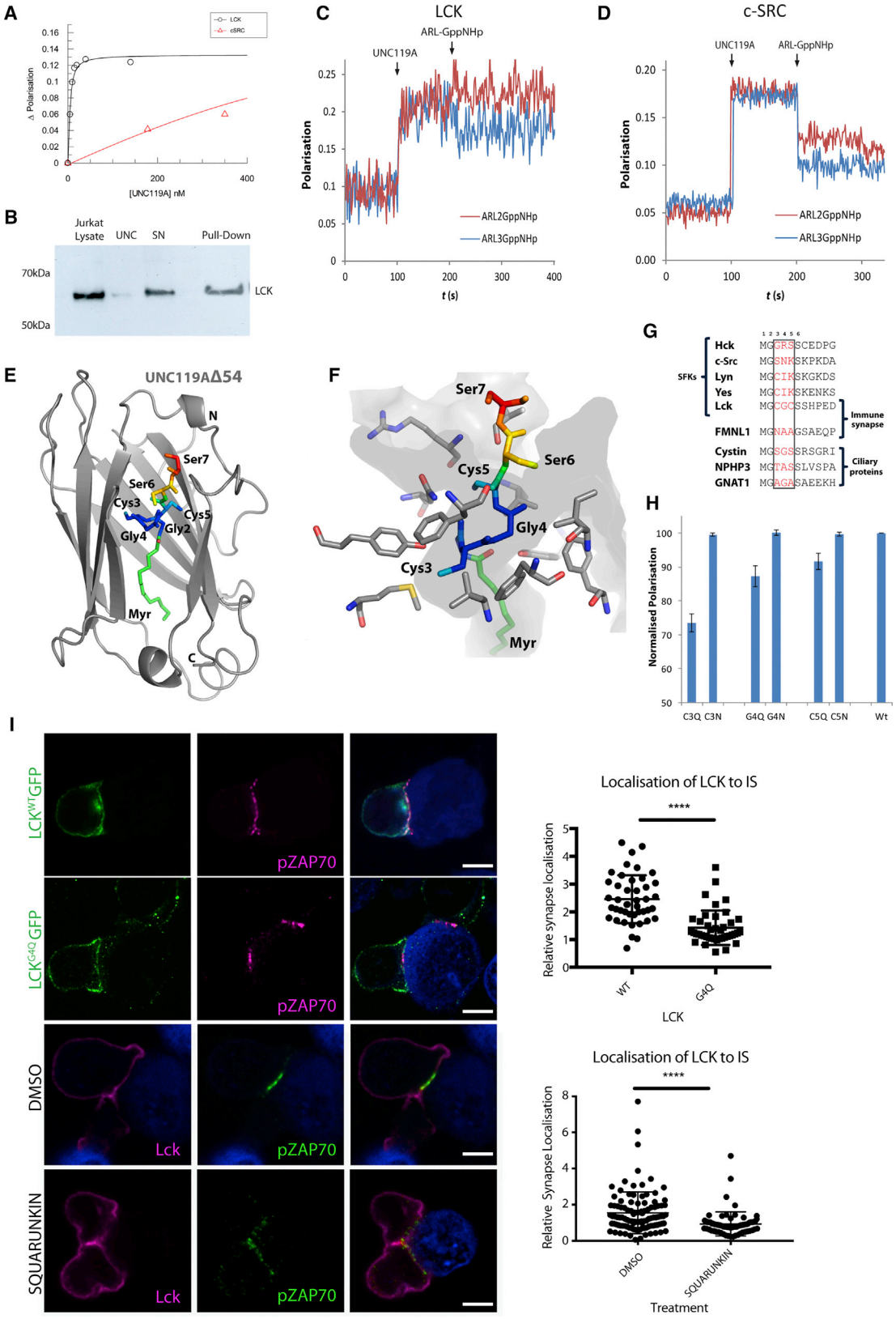

(legend on next page)

UNC119A. We probed this specificity by measuring the binding affinity constants of UNC119A to LCK or c-SRC using fluorescently labeled myristoylated N-terminal peptides in fluorescence polarization experiments. The myristoylated LCK peptide bound to UNC119A with more than 50-fold binding affinity compared to c-SRC (ca 2 nM and 125 nM, respectively) (Figure 1A). This demonstrates a clear specificity for UNC119A toward LCK. Furthermore, using recombinant GST-tagged UNC119A, we were able to pull down LCK from Jurkat T-cell lysate (Figure 1B).

The GTP-bound form of the ciliary small G protein ARL3 (but not its non-ciliary homolog ARL2) allosterically disrupts the UNC119A interaction with myristoylated ciliary proteins by the formation of a fast-dissociating ternary complex (Ismail et al., 2012). We performed fluorescence polarization assays, as above, in the presence of ARL3-GTP or ARL2-GTP, to probe disruption of LCK/UNC119A. Only ARL3-GTP was able to disrupt the interaction of the myristoylated LCK peptide with UNC119A, shown by a decrease in the level of polarization (Figure 1C). The UNC119A-c-SRC complex was disrupted by both ARL3-GTP and ARL2-GTP, supporting that LCK (but not c-SRC) is a specific substrate for UNC119A (Figure 1D). To confirm the allosteric mechanism of ARL3 displacing the myristoylated LCK peptide bound to UNC119A, we titrated in ARL3-GTP and ARL2-GTP to a preformed LCK-UNC119A complex. Only ARL3-GTP, and not ARL2-GTP, displaced the bound fluorescently labeled LCK (Figure S1A, left). Nevertheless, ARL3-GTP was not able to completely displace the bound LCK peptide, which opposes a pure competitive model. This result supports the formation of a ternary complex, where ARL3 binds to UNC119A and not LCK, with reduced affinity to myristoylated LCK (Figure S1A, right). Thus, we established that UNC119A interacts with high affinity and specificity toward LCK and that this complex is specifically disrupted by the ciliary ARL3-GTP, potentially implicating LCK in a ciliary trafficking pathway.

LCK-UNC119A High-Affinity Binding Confers Localization at the Immune Synapse

To gain atomic-level insight into the specificity of UNC119A toward LCK, we solved the crystal structure of a myristoylated LCK peptide in complex with UNC119A (54-240) at 2-Å resolution (Figure 1E and Table S1). The asymmetric unit had three molecules of UNC119A in complex with the myristoylated LCK peptide. The first four amino acids of the myristoylated LCK were well ordered and superimposed well in the three complexes in the asymmetric unit (Figures S1B and S1C). Amino acids beyond the fourth residue were not visible in the electron density map, except in only one complex molecule where amino acids 5 and 6 were visible (Figure S1B). UNC119A shows the expected beta sandwich immunoglobulin conformation and the myristoyl group and the first three amino acids from the unique domain of LCK are buried deep inside the UNC119A hydrophobic pocket (Figures 1E and 1F). The myristoylated peptide superimposes well with the reported crystal structure of the ciliary myristoylated NPHP3 peptide in complex with UNC119A (Jaiswal et al., 2016) (Figure S1D). Sequence alignment of reported myristoylated ciliary UNC119A interactors and LCK do not show any large residues at positions 3, 4, and 5 (Zhang et al., 2011) (Figure 1G). The structure shows limited space around cysteine 3 and glycine 4, where large amino acids would result in a steric clash; however, there is more space around cysteine 5 (Figure 1F). To test the importance of having a small residue at these positions, we took advantage of the fact that ARL2-GTP can only displace lower binding affinity cargo bound to UNC119A. We performed fluorescence polarization assays in which we probed the ability of ARL2-GTP, at saturating concentrations, to disrupt the interaction of UNC119A to different mutated LCK myristoylated peptides with a large amino acid (glutamine) introduced at positions 3, 4, or 5. The introduction of a glutamine residue at these positions resulted in the ability of ARL2-GTP to disrupt the UNC119A-peptide complex. To compare the impact of introducing a large amino acid between positions 3, 4, and 5, we measured the ability of ARL2-GTP to disrupt the respective complexes by monitoring the fractions of the peptide that are released, which are indicated by the drop in the polarization signal, under similar conditions. Position 3 had the most impact, followed by 4 and then 5. Furthermore, to test the impact of the size of the amino acid on the disruption of the complex, we repeated this experiment with a smaller amino acid (asparagine), where we did not observe any release by ARL2-GTP (Figure 1H).

Figure 1. High Affinity of Myristoylated LCK to UNC119A: Structural Basis, ARL3-Specific Release, and Effect on Cellular Localization

(A) Increasing concentrations of full-length UNC119A were titrated against 5-nM fluorescein-labeled myristoylated LCK (black) or 0.5-μM c-SRC (red) peptides, and the resultant increase in fluorescence polarization was plotted against the concentration of UNC119A. Binding affinities for LCK and c-SRC were calculated as 2.2 ± 0.7 nM and 125 ± 69 nM, respectively.

(B) Western immunoblot where 30-μg GST-tagged full-length UNC119A was used in a pull-down with Jurkat T cells lysate. SN, supernatant; UNC, negative control.

(C and D) Fluorescence polarization measurement, where 10-nM (C) or 0.5-uM (D) full-length UNC119A was added to 5-nM LCK (Myr-GCGCSSHPED) (C) or 0.5-μM c-SRC (Myr-GSNKSKPKDASQ) fluorescein-labeled myristoylated peptides followed by the addition of GppNHp-ARL2 (red) or -ARL3 (blue) as indicated.

(E) Crystal structure of UNC119AΔ54 (gray) in a complex with a myristoylated LCK peptide with the myristoyl group in green and the peptide in blue to red, indicating increasing B-factors.

(F) Surface representation of the UNC119A pocket (gray) enclosing the myristoyl moiety (green) and LCK peptide (blue to red, increasing B-factors). UNC119A residues that can potentially clash with a bulky residue in LCK peptide (positions 3, 4, and 5) are shown in stick representation (gray).

(G) Sequence alignment of known ciliary UNC119A cargo proteins and examples of SRC family kinases (SFKs).

(H) 500-nM GppNHp-loaded ARL2 was added to a mixture of 100-nM UNC119A and 100-nM fluorescein-labeled N-terminal peptides of wild-type and mutant LCK, and the resulting drop in fluorescence polarization was measured (the y axis represents the polarization signal normalized to the maximum increase in polarization prior to the addition of ARL2-GppNHp) (the experiment was repeated three times and standard deviations are presented as error bars, from left to right: 2.64, 0.46, 3.13, 0.86, 2.42, 0.52, and 0.06).

(I) Jurkat T cells were nucleofected with either wild-type (LCK^{WT}GFP) or low-affinity mutant LCK (LCK^{G4Q}GFP) (left). T:B cell conjugates were produced using Jurkat T cells and Raji B cells incubated in SEE and CMAC (blue). Relative synapse localization (localization ratio, LR) of LCK^{WT}GFP (n = 45) is 2.45, and that of LCK^{G4Q}GFP (n = 42) = 1.4. Mann-Whitney $p \leq 0.0001$. Scale bars, 5 μm. On the right side, T cells were treated with either DMSO or squarunkin A, a UNC119A inhibitor. DMSO-treated cells (n = 105) showed LCK LR = 1.54 and squarunkin A-treated cells (n = 71) LCK LR = 0.94 Mann-Whitney $p \leq 0.0001$. Scale bars, 5 μm. See also Figure S1.

Sequence alignment of the first six amino acids of all SFKs shows LCK to be the only member that does not have a large amino acid at positions 3, 4, and 5. To confirm our results, we performed pull-down experiments, using GST-UNC119A as bait, following *in vitro* myristoylation, by adding myristoyl-CoA and the enzyme N-myristoyltransferase to the unique-SH3-SH2 domains of HCK and FYN, in the presence and absence of ARL2-GTP or ARL3-GTP. As expected, ARL2 was able to disrupt the interaction of HCK and FYN to UNC119A (Figure S1E). Furthermore, HCK has an arginine residue at position 4 and small amino acids at positions 3 and 5; thus, we mutated this residue into the small amino acid glycine. Contrary to wild-type myristoylated HCK, which is released by both ARL2- and ARL3-GTP (Figure S1F, lanes 2 and 3), the myristoylated HCK^{R4G} mutant was only released by ARL3-GTP and not ARL2-GTP as in the case of LCK, confirming our findings (Figure S1F, lanes 8 and 9). From our experiments on LCK, we concluded that the absence of large residues at positions 3, 4, and 5 is critical for a high-affinity binding interaction with UNC119A.

To investigate the significance of the affinity in the localization and specific release of LCK by ARL3, we expressed the low-affinity mutant, LCK^{G4Q}GFP in Jurkat T cells and analyzed its localization to a staphylococcal E enterotoxin (SEE)-induced synapse. The LCK^{G4Q} mutant is released by ARL3-GTP and ARL2-GTP, due to weakening of the interaction with UNC119A as seen from the structure (see above). We calculated the relative localization of LCK^{WT}GFP and LCK^{G4Q}GFP to the immune synapse by producing T-B cell conjugates, whereby the T cells were nucleofected with the LCK-GFP constructs and B cells incubated with the superantigen, SEE. The localization of the GFP-tagged proteins to the immune synapse, relative to the rest of the cell, was calculated using the ImageJ plug-in ''immune synapse measures,'' and this localization was assigned a localization ratio (LR) of 0, there being no localization (Calabia-Linares et al., 2011). While LCK^{WT}GFP shows an LR = 2.45, similar to that identified for endogenous LCK (Figure 3A), LCK^{G4Q}GFP fails to localize efficiently to the synapse (LR = 1.4; Figure 1I).

To corroborate this finding, we analyzed the localization of LCK to SEE-induced synapse in the presence of the selective UNC119-cargo inhibitor squarunkin A, which blocks the UNC119A myristoyl binding pocket, thus inhibiting its interaction with LCK (Mejuch et al., 2017). The localization of endogenous LCK in the immune synapse was calculated relative to the rest of the cell, as above. While LCK localization in the presence of DMSO shows an LR = 1.54, relative localization in the presence of squarunkin A was reduced to 0.94 (Figure 1I). These experiments demonstrate the importance of the high-affinity binding of LCK to UNC119A to enable correct localization and enrichment at the immune synapse.

A Motif for UNC119A-Mediated Trafficking to the Immune Synapse and Cilium

To investigate whether the structural requirement might enable cargo prediction based on amino acid sequence, we searched in the protein database for additional proteins with a myristoylation signal and without large residues at positions 3, 4, and 5. Among the proteins identified were the ciliary proteins cystin, NPHP3, and GNAT1, as well as the formin-like protein FMNL1, which was reported to localize at the immune synapse (Gomez et al., 2007). FMNL1 was pulled down from Jurkat T cells by GST-UNC119A, and specific treatment of the interaction with ARL3-GTP released FMNL1 (Figure 2A). Fluorescence polarization experiments using N-terminal FMNL1 peptides confirmed that FMNL1 interacts with UNC119A with a high affinity compared to its homolog FMNL3 and is specifically released from UNC119A by ARL3-GTP (Figures 2B–2D). Titrating ARL2 and ARL3 into a solution of UNC119A-FMNL1 peptide complex resulted in FMNL1 release only in the case of ARL3 (Figure 2E). These experiments suggest FMNL1 as a potential cargo protein for UNC119A and further support the notion that cilia and immune synapses share common features (de la Roche et al., 2016). Thus, from our structural work, we were able to predict a potential cargo of UNC119A and provide a basis for the specificity toward certain cargoes. We defined a motif, comprising the myristoylation consensus sequence (PDOC00008-PROSITE) + a small or medium size amino acid at positions 3, 4, and 5, for UNC119A high-affinity binding that we name ''UNC119A Specific Cargo'' (USC) sequence.

Activation of ARL3 and Release of LCK at the Immune Synapse

To investigate the activation and localization of ARL3 in comparison to LCK at the immune synapse, we used T-B cell conjugates, whereby Jurkat T cells were added to Raji B cells incubated with the superantigen, SEE, and the position of the synapse identified by phosphorylated ZAP70 (pZAP70) (Figure 3A, green). ARL3 appeared to be dispersed throughout the cell, whereas LCK was focused at the immune synapse. If ARL3 is the release factor of UNC119A, it is likely that ARL3-GTP is focused at the synapse to allow specific release. To test this possibility, we expressed a constitutively active mutant form of the protein ($ARL3^{Q71L}$). When Jurkat T cells were nucleofected with $ARL3^{WT}$GFP, LCK localized to the immune synapse (LR = 2), comparable to the localization of LCK^{WT}GFP (LR = 1.9; Figure 1I). However, expression of $ARL3^{Q71L}$, which is active throughout the cell, resulted in a significant reduction in the localization of LCK to the immune synapse to LR = 1.09 (Mann-Whitney p = 0.0002) (Figures 3C and 3D). Thus, precise activation of ARL3 at the immune synapse is crucial for release of LCK. To measure the impact of the $ARL3^{Q71L}$ on T cell signaling, we looked at expression of CD69 as a marker of stimulation in Jurkat T cells, transfected with the same constructs and stimulated with anti-CD28 and CD3 antibodies and analyzed using flow cytometry. Strikingly, expression of $ARL3^{Q71L}$GFP resulted in the increased expression of CD69 (Figure 3E). When CD69 expression in transfected cells was normalized to 1 in GFP-transfected cells, $ARL3^{WT}$GFP showed no significant change in stimulation, while $ARL3^{Q71L}$GFP stimulation was increased by a factor of 2 (Figures 3E and S4A). Interestingly, when the non-ciliary release factor, $ARL2^{WT}$GFP, and its constitutively active mutant, $ARL2^{Q70L}$GFP, were transfected into cells, we saw no alteration in T cell activation (Figures 3E and S4B). Thus, ARL3, previously thought to be a specific cilia release factor, is clearly an essential component of the regulation of the immune synapse, lending further support to the hypothesis that the immune synapse is a modified cilium and that LCK trafficking is a central part of its function.

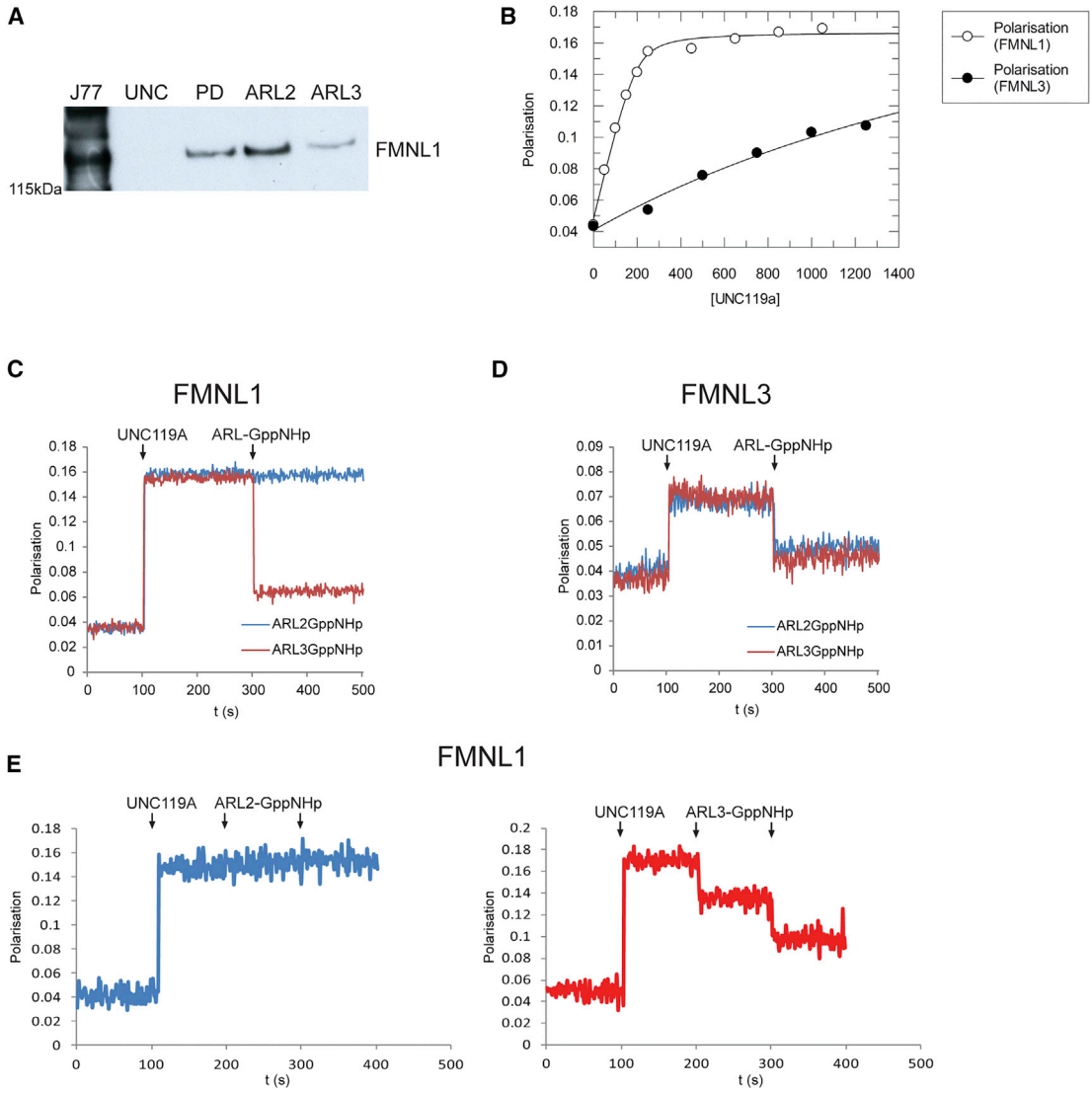

Figure 2. FMNL1 Is a High-Affinity Cargo for UNC119A

(A) Western immunoblot where 30-μg GST-tagged full-length UNC119A was used to pull down Jurkat lysate in the presence or absence of 30-μg ARL2GppNHp or ARL3GppNHp.

(B) Full-length UNC119A was titrated into a solution of 0.2-μM fluorescein-labeled myristoylated FMNL1 (○) or FMNL3 (•) peptides. Binding affinities for FMNL1 and FMNL3 were calculated as 10.1 ± 3.5 nM and 856 ± 156 nM, respectively.

(C and D) Fluorescence polarization measurement where 0.5-μM full-length UNC119A was added to 0.5-μM fluorescein-labeled myristoylated FMNL1 (C, Myr-GNAAGSAEQPAG) or FMNL3 (D, Myr-GNLESAEGVPGE) peptide followed by 5-μM GppNHp-loaded ARL2 or ARL3.

(E) GppNHp-loaded ARL2 and ARL3 were added in 2.5-μM steps to a mixture of 0.5-μM fluorescein-labeled myristoylated FMNL1 peptide and 0.5-μM UNC119A as indicated.

We then asked the question: what activates ARL3 at the immune synapse? In cilia, ARL13B has been shown to function as a GEF for ARL3 (Gotthardt et al., 2015). ARL13B is reported to localize exclusively in cilia; however, lymphocytes are among the few cell types that do not possess cilia. Endogenous ARL13B and LCK were seen sparsely throughout the membrane of the unstimulated cell (Figures 3A and 3F; SEE^{-}). ARL13B has not previously been identified in non-ciliated cells, so we hypothesized that T cells were co-opting this ciliary pathway at the immune synapse. UNC119A has previously been shown to localize to the immune synapse in Jurkat T cells (Gorska et al., 2004); however, ARL13B has not been studied in this system. Upon its formation of the immune synapse, the immune synapse shows a striking focusing of ARL13B that is similar to LCK (Figure 3F, red). To confirm our observation, we quantified the ratio of fluorescence intensity at the immune synapse compared to that in the rest of the cell membrane. While localization of ARL3 showed a ratio of 0.2 that did not change after stimulation, ARL13B and LCK showed ratios of 0.7 (ARL13B) and 0.8 (LCK) in the unstimulated state, significantly increased (Mann-Whitney $p \leq 0.0001$) in the presence of SEE to 2.1 (ARL13B) and 1.8 (LCK) (Figure 3B). The specificity of ARL13B localization at the immune

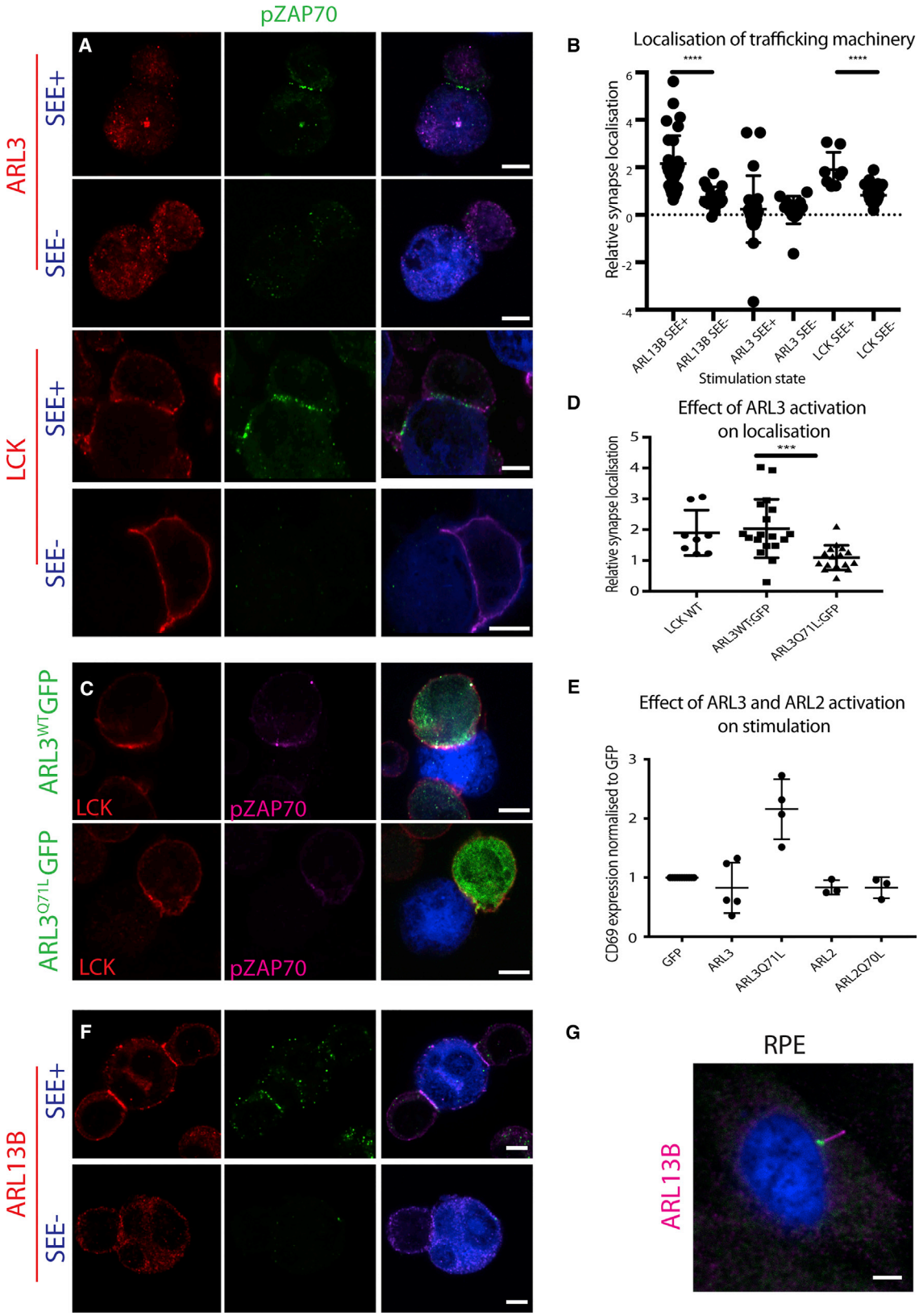

(legend on next page)

synapse shares a striking resemblance to that of ciliary localization in retinal pigment epithelial (RPE) cells (Figures 3F and 3G), again supporting the notion that cilia and immune synapses share common features.

UNC119A Regulatory Arm Interacts with LCK Kinase Domain

The myristoyl group is required for LCK to anchor to membranes and mediates the interaction with UNC119A. Therefore, UNC119A will not be able to interact with the lipid group unless LCK is dissociated from the membrane. Given the high concentration of membranes in the cell, an interaction interface additional to the myristoyl group would facilitate the interaction of LCK with UNC119A and thus aid its extraction from membranes. To investigate the possibility of another interaction site between UNC119A and LCK, we performed pull-down experiments using full-length constructs of UNC119A and non-myristoylated LCK. Indeed, recombinant non-myristoylated LCK was pulled down using GST-UNC119A as bait (Figure 4A, lane 1). On further investigation, full-length UNC119A was able to interact, albeit weakly, with only the kinase domain of LCK, as seen by pull-down experiments using an LCK construct lacking the unique, SH3 and SH2 domains (Figure 4B, lane 1). LCK constructs comprising the N-terminal domains and excluding the kinase domain were not pulled down by UNC119A, both full-length and Δ54 (Figure S2A).

Rho guanosine nucleotide dissociation inhibitors (GDIs) are a class of proteins that bind to lipid-modified Rho proteins. The immunoglobulin-like β sandwich fold of Rho GDIs binds to the lipid group of their cognate Rho proteins, whereas their N terminus forms a regulatory arm that contacts the Rho switches regions (Figure S2B). The Rho GDI regulatory arm senses the activity status of their cognate Rho proteins (i.e., GTP- or GDP-bound) and facilitates their extraction from membranes (Hoffman et al., 2000). Since Rho GDIs superimpose structurally well with UNC119A Δ54, we hypothesized that UNC119A might act similarly to Rho GDI (Figure S2B). However, the N-terminal first 54 amino acids of UNC119A were not included in the crystallized construct as they hindered crystallization and so, to test if the N terminus of UNC119A contacts LCK, we compared full-length UNC119A and UNC119A-Δ54 in their ability to interact with non-myristoylated LCK; only full-length showed binding (Figure 4A, lanes 1 and 2). To further test this observation, we performed the same experiment using the UNC119A paralog UNC119B, which has a different N terminus. UNC119B did not interact with non-myristoylated LCK (Figure 4A, lane 3). Additionally, we tested the interaction of UNC119A with non-myristoylated c-SRC; very little interaction was detected compared to that of LCK as seen by pull-down experiments, confirming the specificity of UNC119A toward LCK (Figure S2C, lanes 1 and 3). Neither showed pull-down with N-terminally truncated UNC119A-Δ54 (Figure S2C, lanes 2 and 4).

A UNC119A mutation at glycine position 22 (G22V) has been previously reported in a patient with idiopathic CD4 lymphopenia (ICL) (Gorska and Alam, 2012). This mutation was reported to disrupt the interaction of UNC119A with LCK, resulting in the localization of the latter on the endosomes and reducing the amount of LCK on the plasma membrane (Gorska and Alam, 2012). Since glycine 22 is present in the regulatory arm, we wondered if this mutation abrogated the regulatory arm-LCK interaction rather than the hydrophobic pocket interaction with the myristoylated unique domain. Indeed, UNC119A^{G22V} interacted with the myristoyl group of LCK in a fluorescence polarization assay using fluorescently labeled myristoylated LCK N-terminal peptide (Figure S2D). On carrying out a pull-down experiment with UNC119A^{G22V}-GST and full-length, non-myristoylated LCK, no binding was observed (Figure S2E, lanes 1 and 2). This result underscores the importance of the interaction of the regulatory arm with the kinase domain. The localization of LCK to the endosome in the G22V patient mutation supports our proposed model in which UNC119A is recruited to LCK by interaction with its kinase domain, where it extracts it from membranes and deposits it at the desired destination (plasma membrane).

Phosphorylation of LCK Y394 Inhibits Its Interaction with UNC119A Regulatory Arm and Focuses It at the Immune Synapse

Although activation of LCK by phosphorylation at tyrosine 394 results in a 2-fold increase in activity *in vitro*, in cells it has been shown to be critical for the kinase activity (Hui and Vale, 2014; Liaunardy-Jopeace et al., 2017). Furthermore, it was shown that phosphorylation of tyrosines 394 and 505 on LCK regulates its clustering on plasma membrane (Rossy et al., 2013). Activated LCK is localized at the immune synapse, not the endosomes, as we confirm using anti pY394 antibody on conjugates, in agreement with previous reports (Figure 4C). Here, we investigated whether there is an additional layer of regulation involved in the activation of LCK. We pre-incubated LCK with ATP before performing pull-down experiments using full-length UNC119A and non-myristoylated LCK. Strikingly,

Figure 3. ARL3-Specific Release Localizes LCK to the Immune Synapse

(A and F) T:B cell conjugates stained with anti ARL3, LCK, or ARL13B antibodies as indicated in the presence or absence of SEE.

(B) LR of ARL3, ARL13B, and LCK of conjugates from (A) and (F): ARL3 shows no localization to the synapse in the presence (LR = 0.3) or absence of SEE (n = 38). LCK shows LR = 1.9 in the presence of SEE and 0.7 in its absence (n = 42; $p \leq 0.0001$). ARL13B shows LR = 2 in the presence of SEE (n = 32) and 0.6 in its absence (n = 16; $p \leq 0.0001$).

(C) ARL3^{WT}GFP and the constitutively active ARL3^{Q71L}GFP were nucleofected into cells and T:B cell conjugates, in the presence of SEE, were stained with anti LCK antibodies.

(D) LR of LCK of conjugates from (C). ARL3^{WT}GFP expression had little effect on LR of LCK (n = 18) compared to cells not expressing ARL3^{WT}GFP (LR = 2). ARL3^{Q71L}GFP-expressing cells showed LR of LCK = 1 (n = 16, p = 0.0002). Differences in LR were analyzed using the Mann-Whitney U test (B and D).

(E) CD69 expression was analyzed via flow cytometry for cells stimulated with anti CD28 and CD3 antibodies and overexpressing ARL2-GFP, ARL2^{Q70L}GFP, ARL3^{Q71L}GFP, ARL3-GFP, or GFP. ARL3^{Q71L}GFP ($p \leq 0.0001$), ARL3^{WT}GFP (p = 0.004), ARL2^{WT}GFP (p = 0.02), and ARL2^{Q70L}GFP (p = 0.03) p values refer to unpaired t test data.

(G) Ciliated RPE cell stained with anti ARL13B antibody.

Scale bars, 5 μm.

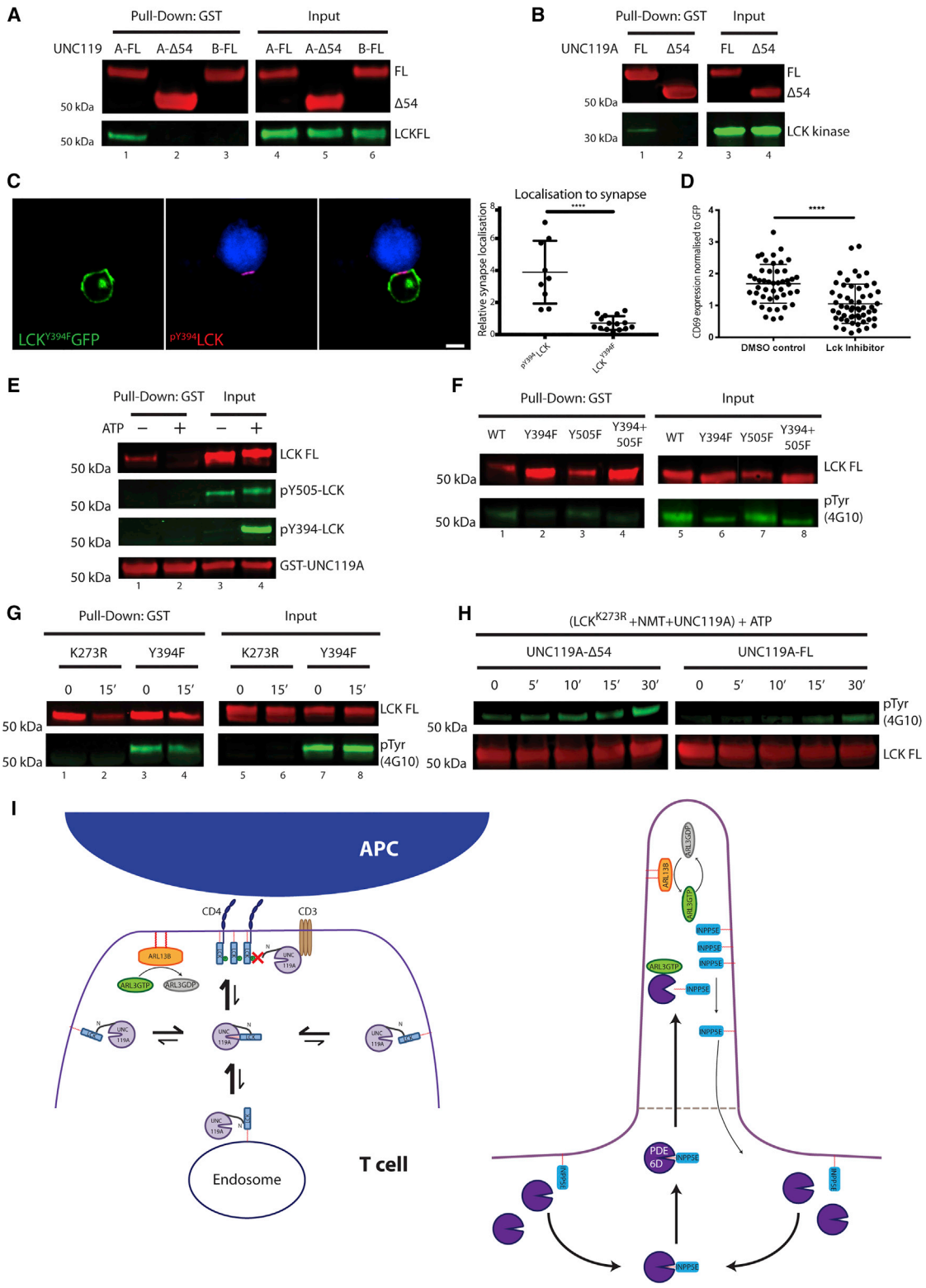

Figure 4. Phosphorylation Regulates the UNC119A N-Terminal Regulatory Arm Interaction with the Kinase Domain of LCK

(A and B) 30 μg of GST-tagged UNC119A-FL (A and B), UNC119A-Δ54 (A and B), and UNC119B-FL (A) were used to pull down 2 μg of non-myristoylated, full-length LCK (A) or 12 μg of purified His-tagged LCK kinase domain (225–509) (B). The proteins were detected by immunoblotting using antibodies against His and GST.

(legend continued on next page)

the addition of ATP abolished the interaction, suggesting that a phosphosite may regulate the interaction (Figure 4E, lanes 1 and 2). We then performed mass spectrometry analysis to identify which phosphosite results in inhibition of the interaction. Mass spectrometry analysis showed several phosphorylated tyrosines upon incubation with ATP. To minimize the effect of non-specific phosphorylation, we used the LCK^{K273R} mutant, which has significantly less kinase activity compared to wild-type LCK (Figure S3B). During pull-down experiments using this mutant in the absence of ATP, we observed a stronger interaction of UNC119A with LCK, as indicated by a stronger LCK band in the LCK^{K273R} pull-down compared to that of the wild-type protein (Figure S3C, lanes 1 and 2). Pre-incubation with 1 mM ATP for 15 min at room temperature inhibited the interaction, thereby supporting the observation that autophosphorylation inhibits the interaction of LCK with UNC119A (Figure S3D, left). Mass spectrometry analysis was carried out for the K273R mutant under the same conditions that resulted in the abrogation of interaction with UNC119A. The analysis showed the phosphorylation of three tyrosine residues: Y181, Y394, and Y489 (Figure S3D, right). We mutated each of these tyrosine residues as well as several others predicted to be phosphorylation sites to phenylalanine and repeated the pull-down experiments to screen for a mutant that showed strong binding to UNC119A despite being phosphorylated on other sites. The mutant residue in this case would likely have a role in regulating the interaction between UNC119A and LCK. All mutants were highly phosphorylated, as seen by anti-phosphotyrosine antibody staining; however, LCK^{Y394F} showed the strongest binding compared to LCK^{WT}, LCK^{K273R}, and the other mutants (Figures 4F [lane 2], S3E, and S3F). Incubation of LCK^{Y394F} with ATP did not abolish the interaction with UNC119A compared to the significantly less active K273R mutant (Figure 4G, lanes 2 and 4). We therefore conclude that it is the phosphorylation of tyrosine 394 that inhibits the interaction of UNC119A regulatory arm with the kinase domain of LCK.

If this additional interaction is indeed inhibited by the phosphorylation of tyrosine 394, we wanted to investigate whether this UNC119A interaction had an effect on the kinase activity of LCK, through tracking its autophosphorylation over time. We incubated LCK^{K273R}, to start with an unphosphorylated LCK population, with ATP following *in vitro* myristoylation in the presence of full-length UNC119A or UNC119A-Δ54. LCK^{K273R} incubated with UNC119A-Δ54 showed increased autophosphorylation as seen upon staining with an anti-phosphotyrosine antibody, whereas incubation with full-length UNC119A showed reduced autophosphorylation (Figure 4H). We therefore conclude that UNC119A interacts with LCK and blocks its autophosphorylation.

To further investigate the effects of LCK phosphorylation at Y394, we produced a GFP-tagged version of LCK^{Y394F}, LCK^{Y394F}GFP and followed its localization upon stimulation of the immune synapse. While LCK^{WT}, as discussed above, localizes to the synapse within 5 min of synapse induction and with an LR = 2.45 (Figure 4C), LCK^{Y394F}GFP fails to localize to the synapse, producing an LR = 0.72. In comparison, active LCK phosphorylated at Y394 and has an LR = 3.89, significantly higher than both LCK^{WT} and LCK^{Y394F} ($p < 0.0001$). Since LCK Y394 undergoes trans-autophosphorylation, we wanted to investigate the effect of inhibiting LCK kinase activity on its enrichment at the immune synapse. For this, we followed the localization of LCK upon the formation of immune synapse in the presence of the selective LCK inhibitor (CAS 213743-31-8) or DMSO control (LR = 1.68). In the presence of the inhibitor, LCK failed to focus at the immune synapse (LR = 1.05). (Figure 4D). These results provide a strong indication that LCK phosphorylation and activity is required for its enrichment at the immune synapse, drawing strong links between activity phosphorylation and localization.

DISCUSSION

LCK associates with CD4 on intracellular membranes within 10 min after synthesis and is transported to the plasma membrane by vesicular trafficking (Bijlmakers and Marsh, 1999). However, when cells were treated with brefeldin A, a fraction of LCK was still able to localize at the plasma membrane, and the authors suggested another direct route beside vesicle trafficking (Bijlmakers and Marsh, 1999). Furthermore, using single-molecule fluorescence microscopy, it was shown that a non-vesicular cytosolic fraction of LCK traffics directly to the plasma membrane (Zimmermann et al., 2010). These observations suggest another cytosolic route of transport of LCK to the plasma membrane. Our proposed model would represent a fast route of targeting compared to vesicle trafficking. In cytotoxic T lymphocytes (CTLs), the cSMAC forms in two stages: a fast initial stage, which was proposed to take place via lateral

(C) Jurkat T cells were nucleofected with LCK^{394F}GFP, and SEE-induced conjugates were stained with anti pY394 LCK antibody (red). ^{pY394}LCK showed LR = 3.89, whereas LR of LCK^{394F} = 0.72 ($p < 0.0001$). Scale bars, 5 μm.

(D) In the presence of the LCK inhibitor (CAS 213743-31-8), LCK failed to focus at the immune synapse (LR = 1.05). This was compared to a DMSO-treated control (LR = 1.68). Mann-Whitney $p \leq 0.0001$.

(E and F) 30 μg of full-length UNC119A-GST was used to pull down 2 μg of non-myristoylated, active LCK that was incubated with 1 mM ATP for 6 hr on ice (E) or 3 μg of non-myristoylated full-length LCKWT, LCKY394F, LCKY505F, and LCKY394+505F (F). The white lines indicate irrelevant lanes that were spliced.

(G) 60 μg of full-length UNC119A-GST was used to pull down 12 μg of purified non-myristoylated LCKK273R and LCKY394F before and after incubation with 1-mM ATP for 15 min at room temperature.

(H) 6 μg of purified non-myristoylated LCKK273R was used for *in vitro* myristoylation in the presence of 30 μg of GST-tagged UNC119-Δ54 (left) or UNC119A-FL (right) before incubating with 1-mM ATP. Autophosphorylation of LCK was monitored by taking samples at 0, 5, 10, 15, and 30 min. Proteins on (E) to (H) were detected using antibodies as indicated on the figures.

(I) Left: Myristoylated LCK is extracted from membranes by UNC119A through a regulatory-arm kinase domain interaction as well as hydrophobic pocket-myristoyl group binding. Solubilized LCK can then be transported in the cytosol. Localization of GEFs such as ARL13B at the immune synapse drives activation of ARL3. LCK released by ARL3-GTP can then anchor to the plasma membrane; the reverse process is inhibited by phosphorylation of LCK tyrosine 394 (i.e., activation of LCK). (I) Right: A model of how farnesylated ciliary INPP5E is sorted into the cilium using PDE6D (Fansa et al., 2016).

See also Figures S2–S4.

diffusion, followed by vesicular trafficking (Ritter et al., 2015). Our model might represent an initial fast route to the immune synapse. Another possibility would be UNC119A facilitating the deposition of LCK from endosomal vesicles to the immune synapse, as was previously suggested (Gorska et al., 2009). A role of UNC119A in targeting LCK from both plasma membrane and endosome cannot be excluded, especially based on the co-localization of UNC119A and LCK at both the plasma membrane and endosomes (Figures 4I and S4C).

LCK undergoes co- and post-translational modifications including myristoylation and palmitoylation, which are critical for the localization of LCK on plasma membranes and RAB11-positive endosomes (Gorska et al., 2009; Zlatkine et al., 1997). Palmitoyl acyltransferase DHHC21 has specificity for LCK and is localized on the plasma membrane (Akimzhanov and Boehning, 2015). This supports our model, as it would result in the long-term entrapment of myristoylated and palmitoylated LCK on the membrane. It will be interesting to investigate the palmitoylation-depalmitoylation cycle of LCK in the context of the model we are proposing and whether LCK is maintained at the immune synapse by spatial cycles of solubilization, release, and palmitoylation at the plasma membrane.

Cilia are found on almost all cell types, a rare exception being T cells (Goetz and Anderson, 2010). Nevertheless, similarities between the cilium and immune synapse have recently become an exciting and growing field (de la Roche et al., 2016). For the cilium to concentrate lipid-modified proteins, it uses UNC119A, UNC119B, and PDE6D (Figure 4I). Our results support the notion that the cilia and immune synapses share common mechanistic features.

All proteins involved in the proposed model are involved in ciliopathies, and of particular interest is UNC119A, which has been reported to be involved in a ciliopathy-related, cone-rod dystrophy (Kobayashi et al., 2000). Interestingly, UNC119A has also been reported to be involved in ICL, an immunodeficiency disorder, providing an interesting link between the fields of immunology and cilia research (Gorska and Alam, 2012). Our current study will provide possible links between immune pathologies and ciliopathies and will open the door for further investigations.

STAR★METHODS

Detailed methods are provided in the online version of this paper and include the following:

- KEY RESOURCES TABLE
- CONTACT FOR REAGENT AND RESOURCE SHARING
- EXPERIMENTAL MODEL AND SUBJECT DETAILS
  - Cell Culture
- METHOD DETAILS
  - Plasmid and Proteins
  - Antibodies and Westerns
  - Nucleotide Exchange
  - Myristoylation
  - Pull-Down Assays with Recombinant Proteins
  - *In Vitro* Fluorescence Measurements
  - Crystallization and Structure Solution
  - Kinase Assay
  - Nucleofection
  - LCK Inhibitor Treatment
  - UNC119 Inhibitor Treatment
  - Conjugate Formation
  - Immunofluorescence
  - Microscopy
  - Flow Cytometry
- QUANTIFICATION AND STATISTICAL ANALYSIS
  - Quantification of Proteins to the Immune Synapse
  - T-Cell Stimulation
  - Binding Affinities
- DATA AND SOFTWARE AVAILABILITY

SUPPLEMENTAL INFORMATION

Supplemental Information includes four figures and one table and can be found with this article online at https://doi.org/10.1016/j.devcel.2018.08.012.

ACKNOWLEDGMENTS

We would like to thank Danny Huang, Leo Carlin, Raphael Gasper, and Laura Machesky for the excellent scientific discussions. We want to thank Diamond Light Source (DLS) for access to beamlines I02, I03, and I04−1 that contributed to the results presented here. We thank Sergio Lila from the proteomics group for performing and analyzing the MS experiments; Margaret O'Prey and David Strachan who supported all imaging work; and Tom Gilbey for flow cytometry. This work was supported by Cancer Research UK (CRUK core funding award A19257).

AUTHOR CONTRIBUTIONS

L.A.S., Y.E., and M.J.M. performed all the experiments and their analyses and contributed to their design; T.Y. strongly supported structure determination; P.C.S. and P.R. supported the immunology; S.I. supervised the work, designed the experiments, and wrote the manuscript with L.A.S., Y.E., and M.J.M.

DECLARATION OF INTERESTS

The authors declare no competing interests.

Received: January 22, 2018
Revised: June 13, 2018
Accepted: August 15, 2018
Published: September 13, 2018

REFERENCES

Akimzhanov, A.M., and Boehning, D. (2015). Rapid and transient palmitoylation of the tyrosine kinase Lck mediates Fas signaling. Proc. Natl. Acad. Sci. USA *112*, 11876–11880.

Ballek, O., Valečka, J., Manning, J., and Filipp, D. (2015). The pool of preactivated Lck in the initiation of T-cell signaling: a critical re-evaluation of the Lck standby model. Immunol. Cell Biol. *93*, 384–395.

Bijlmakers, M.J., and Marsh, M. (1999). Trafficking of an acylated cytosolic protein: newly synthesized p56(lck) travels to the plasma membrane via the exocytic pathway. J. Cell Biol. *145*, 457–468.

Boggon, T.J., and Eck, M.J. (2004). Structure and regulation of Src family kinases. Oncogene *23*, 7918–7927.

Calabia-Linares, C., Robles-Valero, J., de la Fuente, H., Perez-Martinez, M., Martín-Cofreces, N., Alfonso-Pérez, M., Gutierrez-Vázquez, C., Mittelbrunn, M., Ibiza, S., Urbano-Olmos, F.R., et al. (2011). Endosomal clathrin drives actin accumulation at the immunological synapse. J. Cell Sci. *124*, 820–830.

Cen, O., Gorska, M.M., Stafford, S.J., Sur, S., and Alam, R. (2003). Identification of UNC119 as a novel activator of SRC-type tyrosine kinases. J. Biol. Chem. *278*, 8837–8845.

de la Roche, M., Asano, Y., and Griffiths, G.M. (2016). Origins of the cytolytic synapse. Nat. Rev. Immunol. *16*, 421–432.

Ehrlich, L.I., Ebert, P.J., Krummel, M.F., Weiss, A., and Davis, M.M. (2002). Dynamics of p56lck translocation to the T-cell immunological synapse following agonist and antagonist stimulation. Immunity *17*, 809–822.

Fansa, E.K., Kösling, S.K., Zent, E., Wittinghofer, A., and Ismail, S. (2016). PDE6δ-mediated sorting of INPP5E into the cilium is determined by cargo-carrier affinity. Nat. commun. *7*, 11366.

Goetz, S.C., and Anderson, K.V. (2010). The primary cilium: a signalling centre during vertebrate development. Nat. Rev. Genet. *11*, 331–344.

Gomez, T.S., Kumar, K., Medeiros, R.B., Shimizu, Y., Leibson, P.J., and Billadeau, D.D. (2007). Formins regulate the actin-related protein 2/3 complex-independent polarization of the centrosome to the immunological synapse. Immunity *26*, 177–190.

Gorska, M.M., and Alam, R. (2012). A mutation in the human uncoordinated 119 gene impairs TCR signaling and is associated with CD4 lymphopenia. Blood *119*, 1399–1406.

Gorska, M.M., Liang, Q., Karim, Z., and Alam, R. (2009). Uncoordinated 119 protein controls trafficking of Lck via the Rab11 endosome and is critical for immunological synapse formation. J. Immunol. *183*, 1675–1684.

Gorska, M.M., Stafford, S.J., Cen, O., Sur, S., and Alam, R. (2004). Unc119, a novel activator of Lck/Fyn, is essential for T cell activation. J. Exp. Med. *199*, 369–379.

Gotthardt, K., Lokaj, M., Koerner, C., Falk, N., Gießl, A., and Wittinghofer, A. (2015). A G-protein activation cascade from Arl13B to Arl3 and implications for ciliary targeting of lipidated proteins. Elife *4*, https://doi.org/10.7554/eLife.11859.

Hoffman, G.R., Nassar, N., and Cerione, R.A. (2000). Structure of the Rho family GTP-binding protein Cdc42 in complex with the multifunctional regulator RhoGDI. Cell *100*, 345–356.

Hui, E., and Vale, R.D. (2014). In vitro membrane reconstitution of the T-cell receptor proximal signaling network. Nat. Struct. Mol. Biol. *21*, 133–142.

Ismail, S.A., Chen, Y.X., Miertzschke, M., Vetter, I.R., Koerner, C., and Wittinghofer, A. (2012). Structural basis for Arl3-specific release of myristoylated ciliary cargo from UNC119. EMBO J. *31*, 4085–4094.

Jaiswal, M., Fansa, E.K., Kösling, S.K., Mejuch, T., Waldmann, H., and Wittinghofer, A. (2016). Novel biochemical and structural insights into the interaction of myristoylated cargo with Unc119 protein and their release by Arl2/3. J. Biol. Chem. *291*, 20766–20778.

Kobayashi, A., Higashide, T., Hamasaki, D., Kubota, S., Sakuma, H., An, W., Fujimaki, T., McLaren, M.J., Weleber, R.G., and Inana, G. (2000). HRG4 (UNC119) mutation found in cone-rod dystrophy causes retinal degeneration in a transgenic model. Invest. Ophthalmol. Vis. Sci. *41*, 3268–3277.

Liaunardy-Jopeace, A., Murton, B.L., Mahesh, M., Chin, J.W., and James, J.R. (2017). Encoding optical control in LCK kinase to quantitatively investigate its activity in live cells. Nat. Struct. Mol. Biol. *24*, 1155–1163.

Mejuch, T., Garivet, G., Hofer, W., Kaiser, N., Fansa, E.K., Ehrt, C., Koch, O., Baumann, M., Ziegler, S., Wittinghofer, A., et al. (2017). Small-molecule inhibition of the UNC119-cargo interaction. Angew. Chem. Int. Ed. *56*, 6181–6186.

Monks, C.R., Freiberg, B.A., Kupfer, H., Sciaky, N., and Kupfer, A. (1998). Three-dimensional segregation of supramolecular activation clusters in T cells. Nature *395*, 82–86.

Nika, K., Soldani, C., Salek, M., Paster, W., Gray, A., Etzensperger, R., Fugger, L., Polzella, P., Cerundolo, V., Dushek, O., et al. (2010). Constitutively active Lck kinase in T cells drives antigen receptor signal transduction. Immunity *32*, 766–777.

Padovani, D., Zeghouf, M., Traverso, J.A., Giglione, C., and Cherfils, J. (2013). High yield production of myristoylated Arf6 small GTPase by recombinant N-myristoyl transferase. Small GTPases *4*, 3–8.

Philipsen, L., Reddycherla, A.V., Hartig, R., Gumz, J., Kästle, M., Kritikos, A., Poltorak, M.P., Prokazov, Y., Turbin, E., Weber, A., et al. (2017). De novo phosphorylation and conformational opening of the tyrosine kinase Lck act in concert to initiate T cell receptor signaling. Sci. Signal. *10*, https://doi.org/10.1126/scisignal.aaf4736.

Ritter, A.T., Asano, Y., Stinchcombe, J.C., Dieckmann, N.M., Chen, B.C., Gawden-Bone, C., van Engelenburg, S., Legant, W., Gao, L., Davidson, M.W., et al. (2015). Actin depletion initiates events leading to granule secretion at the immunological synapse. Immunity *42*, 864–876.

Rossy, J., Owen, D.M., Williamson, D.J., Yang, Z., and Gaus, K. (2013). Conformational states of the kinase Lck regulate clustering in early T cell signaling. Nat. Immunol. *14*, 82–89.

Zhang, H., Constantine, R., Vorobiev, S., Chen, Y., Seetharaman, J., Huang, Y.J., Xiao, R., Montelione, G.T., Gerstner, C.D., Davis, M.W., et al. (2011). UNC119 is required for G protein trafficking in sensory neurons. Nat. Neurosci. *14*, 874–880.

Zimmermann, L., Paster, W., Weghuber, J., Eckerstorfer, P., Stockinger, H., and Schütz, G.J. (2010). Direct observation and quantitative analysis of Lck exchange between plasma membrane and cytosol in living T cells. J. Biol. Chem. *285*, 6063–6070.

Zlatkine, P., Mehul, B., and Magee, A.I. (1997). Retargeting of cytosolic proteins to the plasma membrane by the Lck protein tyrosine kinase dual acylation motif. J. Cell Sci. *110*, 673–679.

STAR★METHODS

KEY RESOURCES TABLE

REAGENT or RESOURCE	SOURCE	IDENTIFIER
Antibodies		
anti-His monoclonal	Takara/Clontech	Cat#631212; RRID: AB_2721905
anti-GST polyclonal	GE Healthcare,	Cat#27-4577-01V; RRID: AB_771432
anti-LCK	Sigma-Aldrich	Cat#HPA003494; RRID: AB_1852751
anti-LCK pY505	BD Biosciences	Cat#558552; RRID: AB_397084
anti-LCK pY394	Abcam	Cat#ab201567
anti-FMNL1	Bethyl Laboratories	Cat#A304-869A; RRID: AB_2621064
anti-Phospho-ZAP70 (Y493)	R&D Systems	Cat#MAB7694
IRDye 680RD Donkey Anti-Rabbit IgG (H+L)	Li-Cor	Cat#926-68073; RRID: AB_10954442
IRDye 800CW Donkey Anti-Mouse IgG (H+L)	Li-Cor	Cat#926-32212; RRID: AB_621847
IRDye 680RD Donkey Anti-Goat IgG (H+L)	Li-Cor	Cat# 926-68076; RRID: AB_10956590
CD69 monoclonal antibody (CH/4), APC	ThermoFisher	Cat#MHCD6905; RRID: AB_10372807
Bacterial and Virus Strains		
BL21(DE3)CodonPlus	Agilent Technologies	230245
Chemicals, Peptides, and Recombinant Proteins		
full length c-SRC	Merck/Millipore	14-326
Myr-GCGCSSHPED-OH	JPT peptide technologies	N/A
Myr-GCGCSSHPED-K(5/6-Fluorescein)-amide	Alta Bioscience, University of Birmingham	N/A
Myr-GQGCSSHPED-K(5/6-Fluorescein)-amide	Alta Bioscience, University of Birmingham	N/A
Myr-GCQCSSHPED-K(5/6-Fluorescein)-amide	Alta Bioscience, University of Birmingham	N/A
Myr-GCGQSSHPED-K(5/6-Fluorescein)-amide	Alta Bioscience, University of Birmingham	N/A
Myr-GNGCSSHPED-K(5/6-Fluorescein)-amide	Alta Bioscience, University of Birmingham	N/A
Myr-GCNCSSHPED-K(5/6-Fluorescein)-amide	Alta Bioscience, University of Birmingham	N/A
Myr-GCGNSSHPED-K(5/6-Fluorescein)-amide	Alta Bioscience, University of Birmingham	N/A
Myr-GNAAGSAEQPAG-Fluorescin-amide	Alta Bioscience, University of Birmingham	N/A
Myr-GNLESAEGVPGE-Fluorescin-amide	Alta Bioscience, University of Birmingham	N/A
Critical Commercial Assays		
ProFluor® Src-Family Kinase Assay	Promega	V1270
Deposited Data		
UNC119A-LCK structure	RCSB	6H6A
Experimental Models: Cell Lines		
Jurkat, clone E6-1 cells	ATCC	TIB-152
Raji B cells	DSMZ	ACC 319
RPE	ATCC	CRL-4000
Recombinant DNA		
pET20b-ARL3	This paper	N/A
pET20b-ARL3	This paper	N/A
pET20b-LCK	This paper	N/A
pET20b-LCK(SH3)(1-121)	This paper	N/A
pET20b-LCK(SH3-SH2)(1-226)	This paper	N/A
pET20b-HCK(SH3-SH2)	This paper	N/A
pET20b-Fyn(SH3-SH2)	This paper	N/A
pGEX-4T-1-UNC119A	This paper	N/A
pGEX-4T-1-UNC119B	This paper	N/A
pGEX-4T-1-UNC119A(54-240)	This paper	N/A

(*Continued on next page*)

Continued

REAGENT or RESOURCE	SOURCE	IDENTIFIER
Software and Algorithms		
ImageJ	NIH	https://imagej.nih.gov/ij/index.html
FlowJo software 10.4.2	FlowJo, LLC	https://www.flowjo.com/
Grafit analysis software	Erithacus Software	http://www.erithacus.com/grafit/
Pymol	Schrödinger, LLC	https://pymol.org/2/
Refmac5	CCP4 program Suite	http://www.ccp4.ac.uk/html/refmac5.html
MolRep	CCP4 program Suite	http://www.ccp4.ac.uk/html/molrep.html

CONTACT FOR REAGENT AND RESOURCE SHARING

Further information and requests for resources and reagents should be directed to and will be fulfilled by the Lead Contact, Shehab Ismail (s.ismail@beatson.gla.ac.uk).

EXPERIMENTAL MODEL AND SUBJECT DETAILS

Cell Culture

Jurkat T-cells (Clone E6-1, ATCC,TIB-152, human, male) and Raji B cells (DSMZ, ACC 319, human, male) were maintained in RPMI medium (Thermo Fisher Scientific) with 10% Fetal Calf Serum (FCS). Retinal Pigmented Epithelial (RPE, ATCC, CRL-4000, human, female) cells were maintained and serum starved in DMEM:F12(Thermo Fisher Scientific). All cell lines were grown at 37°C and 5% CO_2.

METHOD DETAILS

Plasmid and Proteins

Full length ARL3 and ARL2 were cloned into pET20b (Novagen) with a C-terminal histidine tag. UNC119A, full length, UNC119A-Δ54 (54-240), and UNC119B, full length were cloned into pGEX-4T-1 (GE Healthcare) with an N-terminal GST tag and purified using a GSTrap HP column (GE Healthcare) followed by size exclusion chromatography. LCK SH3 (residues 1-121), SH3-SH2 (residues 1-226), c-SRC and HCK were cloned in pET20b with C-terminal histidine tags. All histidine tagged constructs were purified using a two-step purification protocol including a nickel affinity His-Trap HP (GE Healthcare) chromatography followed by a size exclusion chromatography. Full-length LCK was cloned in pET20b, expressed in BL21(DE3)CodonPlus *E. coli* cells. Purification was carried out in the same manner as for the shorter constructs, with the addition of 5% glycerol to all purification buffers and increasing the concentration to 20% for storage. Non-myristoylated, full length c-SRC with an N-terminal 6x His-tag was purchased from Merck/Millipore (catalogue number 14-326). The LCK myristoylated peptide (Myr-GCGCSSHPED-OH) was purchased from JPT peptide technologies. pET28(NMT) was a gift from Jim Brannigan.

Antibodies and Westerns

Antibodies used in this study: anti-His monoclonal (Takara/Clontech, 631212), anti-GST polyclonal (GE Healthcare, 27457701V), anti-LCK (Sigma-Aldrich, HPA003494), anti-LCK pY505 (BD Biosciences, 558552), anti-LCK pY394 (Abcam, ab201567). Western blots were imaged using film or using Li-Cor secondary antibodies and visualised on a Li-Cor Odyssey CLX imaging system.

Nucleotide Exchange

400 μM ARL2 or ARL3 was incubated overnight at 15°C with 2 mM of the GTP analogue GppNHp (Jena Bioscience Gmbh) and 69 units of Alkaline phosphatase (Roche). Unbound nucleotides were removed by size exclusion chromatography, using a Superdex 200 Increase column (GE Healthcare). HPLC (UltiMate 3000, ThermoFisher Scientific) analysis using C18 columns was used to determine the concentration of loaded ARL-GppNHp.

Myristoylation

Myristoylation of LCK, c-SRC and HCK was done *in vitro* using recombinant N-myristoyl transferase (NMT) and myristoyl-CoA (Padovani et al., 2013).

Pull-Down Assays with Recombinant Proteins

Pull-downs were typically carried out using 30 μg of GST-tagged UNC119A and 12 μg of LCK in a buffer containing 50 mM Tris (pH 8), 1 mM $MgCl_2$, 1 mM DTT, 0.02% Triton X-100. Reactions including *in vitro* myristoylation also contained 2.5 μM N-myristoyltransferase (NMT) and 100 μM Myristoyl-CoA. Reactions were incubated at room temperature for 3 hours before the addition of

ARL2-GppNHp or ARL3-GppNHp with further incubation at room temperature for 10 minutes. Reactions were then added to Glutathione sepharose 4 FF beads (GE Healthcare) and incubated at room temperature for 20 minutes. Beads were washed 5 times in GF buffer (25 mM Tris (pH 7.5), 200 mM NaCl, 2 mM DTT, and finally proteins were eluted for 10 minutes using GF buffer containing 20 mM Glutathione.

In Vitro Fluorescence Measurements

Fluorescence polarisation measurements were done in a buffer containing 25 mM Tris (pH 7.5), 150 mM NaCl, 5 mM $MgCl_2$ 2 mM DTT. Data were recorded using a QuantaMaster fluorometer (Photon Technology International) with excitation at 490 nm and emission at 520 nm for fluorescein-labelled peptides. Data analysis was done using Grafit 5.0 program (Erithracus software, Horley UK). Fluorescein-labelled LCK wild-type peptide (Myr-GCGCSSHPED-K(5/6-Fluorescein)-amide) and its mutant versions (C3Q, C3N, G4Q, G4N, C5Q, and C5N), as well as FMNL1 (Myr-GNAAGSAEQPAG) and FMNL3 (Myr-GNLESAEGVPGE) peptides were purchased from Alta Bioscience, University of Birmingham.

Crystallization and Structure Solution

A solution of UNC119A-Δ54 at a concentration of 746 μM in a buffer containing 25 mM Tris (pH 7.5), 150 mM NaCl, 2 mM DTT was mixed with pure myristoylated LCK peptide (Myr-GCGCSSHPED-OH) at a 1:1 molar ratio. Crystals appeared in a Qiagen suite PEG (20% w/v PEG 3350, 200 mM KH_2PO_4) at 4°C. Crystals were flash frozen in a solution containing the mother liquor with 25% glycerol. The data were integrated with automated XDS and scaled with the CCP4 suite. Molecular replacement was done with the program Molrep using UNC119A (PDB code 3RBQ) as a search model. Refinement was done by the program Refmac 5 and manual building.

Kinase Assay

Kinase activity of wild-type and mutant versions of LCK was measured using the ProFluor® Src-Family Kinase Assay kit (Promega), as per the manufacturer's instructions and measured using a Tecan Safire 2 multi-mode plate reader (ThermoFisher).

Nucleofection

Jurkat T-cells were nucleofected with ARL3, ARL13B and mutant expression constructs in EGFP N1 using the Amaxa Nucleofector II Kit V (Lonza, Switzerland) as per the instruction manual.

LCK Inhibitor Treatment

Jurkat T-cells were treated with LCK Inhibitor (sc-204052, Santa Cruz Biotechnology, USA) at 0.5 μM in complete medium.

UNC119 Inhibitor Treatment

Jurkat T-cells were treated with 2 μM Squarunkin A (GLXC-10229, Glixx Labs, USA) in complete medium.

Conjugate Formation

Raji B cells were incubated at 10^6 cells/ml for 1 hour in RPMI plus 10 μM CMAC (Life Technologies, USA) and 1 μg Staphylococcal E Enterotoxin (SEE) (Toxin Technologies, USA) for 1 hour at 37°C before washing 3 times in complete medium. Jurkat T-cells were then introduced at a ratio of 1:1 and plated on Poly-L-Lysine (Sigma, UK) coated coverslips (approx. 10^5 per coverslip) and incubated at 37°C for 10 minutes before fixing with ice-cold methanol for 2 minutes followed by several washes in PBS before preparation for immunofluorescence.

Immunofluorescence

Fixed conjugates were incubated in 5% Donkey serum (Sigma, UK) and 0.01% Triton X-100 for 1 hour at room temperature and incubated in primary antibody overnight. The following antibodies were used: anti-Phospho-ZAP70 (Y493) (R&D Systems, USA MAB7694), anti-LCK (Sigma, HPA003494), anti-LCK pY394 (Abcam, ab201567), anti-ARL3 (Proteintech, UK 10961-1-AP), anti-ARL13B (Proteintech, 17711-1-AP), anti-GFP488 (Biolegend, FM264G). RPE cells were fixed in Methanol and immunofluorescence staining carried out as described above. Cilia were identified using anti-ARL13B and anti-γ Tubulin (Sigma, T5192).

Microscopy

Optical sections were taken using the LSM 880 Airyscan or LSM 710 (Zeiss, Germany) and analysed following deconvolution using Fiji (ImageJ). Localisation of proteins to the immune synapse were analysed using the Fiji Plug in Synapse Measures as described by (Calabia-Linares et al., 2011).

Flow Cytometry

Nucleofected Jurkat T-cells were stimulated after 24 hours using an anti-CD3 (UCH-T1, Abcam, ab22) coated 96 well plate and soluble anti-CD28 (BD, Pharmingen, USA, 555726). Cells were stimulated for 4 hours and then analysed using flow cytometry to identify CD69 expression (CD69APC, Invitrogen, USA, MHCD6905). Expression of GFP and APC were measured using the Attune NxT (Thermo Fisher Scientific) and analysed using FlowJo software 10.4.2. The percentage of cells becoming stimulated were calculated and normalised by dividing the percentage of treated cells by that of control cells.

QUANTIFICATION AND STATISTICAL ANALYSIS

Quantification of Proteins to the Immune Synapse

The localisation of proteins to the immune synapse, relative to the rest of the cell was calculated using the ImageJ plug in 'immune synapse measures' and this localisation assigned a localisation ratio (LR), 0 being no localisation. All statistics and n values are included in figure legends.

T-Cell Stimulation

T-cell stimulation was quantified using flow cytometry to identify CD69 expression (CD69APC, Invitrogen, USA, MHCD6905). Expression of GFP and APC were measured using the Attune NxT (Thermo Fisher Scientific) and analysed using FlowJo software 10.4.2. The percentage of cells becoming stimulated were calculated and normalised by dividing the percentage of treated cells by that of control cells. Statistics and n values are included in the relevant figure legend.

Binding Affinities

Binding affinities were calculated by fitting the titation data to a quadratic equation using Grafit analysis software (Erithacus Software). Dissociation constants are provided in the figure legends.

DATA AND SOFTWARE AVAILABILITY

The accession number for the UNC119A-LCK crystal structure reported in this paper is PDB: 6H6A.